Journal of Sol-Gel Science and Technology (2024) 111:718–724
https://doi.org/10.1007/s10971-024-06484-9

ORIGINAL PAPER

Synthesis and characterization of β-spodumene by a new sol–gel route assisted by whey protein

Ricardo Ferrari Ferraz[1] · Maria da Conceição Costa Pereira[2] · Raquel Aline Pessoa Oliveira[1]

Received: 11 June 2024 / Accepted: 4 July 2024 / Published online: 13 July 2024

Abstract

Spodumene ($LiAlSi_2O_6$) has gained attention due to its versatile applications, which include ionizing radiation dosimetry, observed in either monoclinic (α-spodumene) or tetragonal (β-spodumene) symmetries. β-spodumene has been produced by solid-state reactions and conventional sol–gel methods, which are challenging due to the need for high temperatures and costly reagents, respectively. Alternative routes like the Pechini method and proteic sol–gel methods are promising because they can reduce production costs and environmental pollution. This paper aims to synthesize and characterize β-spodumene using a new sol–gel route assisted by whey protein. In this method, proteins act as chelating agents, aiding in the formation of stable colloidal solutions (sol) containing inorganic precursors. These solutions undergo gelation processes to form a solid connected porous structure (gel), which can then be thermally treated to promote crystallization and obtain the desired material. The process involved subjecting the material to thermal treatments exceeding 800 °C, leading to the crystallization of β-spodumene structure at 1000 °C. Additionally, a thermal treatment at 1100 °C facilitated the elimination of residual sulfur (S) resulting from protein combustion. For sample characterizations, thermogravimetric analysis (TGA), differential thermal analysis (DTA), X-ray diffraction (XRD), Fourier transform infrared spectroscopy (FTIR), and X-ray fluorescence (XRF) measurements were performed. Preliminary results indicate that β-spodumene was successfully synthesized using the new sol–gel route assisted by whey protein. The potential of whey protein as an eco-friendly chelating agent is highlighted, suggesting possible environmental benefits and paving the way for future advancements in this research area.

Graphical Abstract

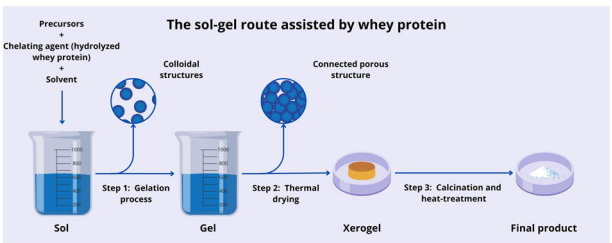

Keywords Eco-friendly · Sol–gel · Spodumene · Whey protein

Highlights

- β-spodumene was effectively synthesized by a new sol–gel route assisted by whey protein.
- Crystalline structure of β-spodumene formed at 1000 °C.
- Eco-friendly approach using whey protein as a chelating agent in the sol–gel method.

✉ Ricardo Ferrari Ferraz
ricardo.univasf@gmail.com

[1] Research Institute of Materials Science (IPCM), Federal University of São Francisco Valley (Univasf), Juazeiro, BA, Brazil

[2] Institute for Energy and Nuclear Research (IPEN), University of São Paulo (USP), São Paulo, SP, Brazil

1 Introduction

Spodumene ($LiAlSi_2O_6$) is a lithium aluminosilicate with significant industrial importance, primarily due to its applications in advanced ceramic materials. Due to its thermoluminescent properties, it has been explored in ionizing radiation dosimetry applications [1, 2]. Depending on temperature and pressure, it has been observed in monoclinic (α-spodumene) or tetragonal (β-spodumene) symmetries [3, 4]. β-spodumene corresponds to the polymorph characterized by its tetragonal crystalline structure, obtained through controlled synthesis or thermal treatment above 850 °C [5]. The choice of β-spodumene as the focus of this investigation stems from its potential as a high-performance material in various applications, given its phase stability and excellent thermal properties make it suitable for use in ceramic pigments, glass additives, and as ionizing radiation sensors [6–10].

The synthesis of this material offers advantages such as controlled properties, purity, homogeneity, cost-effectiveness, and reproducibility. However, conventional synthesis methods such as solid-state reactions often face challenges in achieving homogeneity and require high calcination temperatures. In contrast, the sol–gel approach offers a promising alternative by producing chemically homogeneous materials at lower temperatures compared to those of solid-state reactions [11–15]. Furthermore, the method is often used in the synthesis of zeolites and other porous materials, as it offers significant advantages in creating controlled structures [16]. The potential applications of these materials include catalysis in industrial processes and adsorption and removal of contaminants from water [17–19]. A variant of this route, the proteic sol–gel method, incorporates protein-chelating agents such as coconut water and partially hydrolyzed collagen (gelatin) instead of traditionally used metal alkoxides as precursors. This approach offers advantages in terms of eco-friendliness and cost-effectiveness compared to conventional analytical reagents [20–25].

On the environmental front, cheese whey, a byproduct of cheese production, presents significant challenges due to its high organic matter content and adverse effects on water sources [26]. Whey represents 85–95% of milk volume and retains 55% of milk's nutrients, including lactose, soluble proteins (whey protein), lipids, and minerals [27]. An estimated 180–190 million tons of whey waste are produced globally each year, with 100 million tons originating from cheese whey [28]. This poses a significant environmental concern when discharged into water sources due to its high biochemical oxygen demand (approximately one hundred times the value generated by domestic sewage) [29]. From the perspective of proteic sol–gel synthesis, whey proteins emerge as promising due to the presence of branched-chain essential amino acids (leucine, isoleucine, and valine), which exhibit an affinity for metal ions, capable of forming precursor chelates. However, this application is recent and underexplored, with its first report on the synthesis of ZnO nanoparticles [30].

The present work proposes to produce and verify the effectiveness of whey protein as an innovative and eco-friendly chelating agent in the protein sol–gel technique for the synthesis of β-spodumene, utilizing an unprecedented route for this material. In this study, we analyzed changes in the physical and chemical properties of the xerogel obtained during sample production, the crystalline structure of the material under different heat treatments, and its chemical composition correlation. The findings from this research contribute to advancing the field of aluminosilicate materials science while exploring innovative pathways for utilizing natural proteins in eco-friendly synthesis methodologies.

2 Experimental

2.1 Synthesis

The partially hydrolyzed whey protein powder Hydrovon® 195 (Glanbia Nutritionals Inc/Clean Whey®) was employed as a chelating agent in the process. The protein underwent an initial industrial cross-flow microfiltration process designed to maintain its structural integrity, resulting in a significant reduction in carbohydrate, fat, and metal content. Subsequently, a secondary enzymatic hydrolysis process was employed to cleave the protein into smaller chains, specifically dipeptides and tripeptides. This hydrolysis step is crucial as it facilitates the formation of chelates in the first stage of the sol–gel process. Furthermore, high-purity crystalline silica (SiO_2), with particle size less than 200 mesh, was used as a precursor reagent for silicon, due to its advantages over tetraethoxysilane (TEOS), which is commonly used in the sol–gel technique but carries high cost and toxicity.

Initially, 150 mL of a colloidal suspension (sol) containing a 1:2 weight ratio of chelator to precursors was prepared following the procedure described by Lima et al. [4]. The amount of precursors used corresponds to the stoichiometric ratio for the synthesis of 2 g of β-spodumene per sample: 0.741 g of $LiNO_3$ (Sigma-Aldrich®, 98% purity), 4.032 g of $Al(NO_3)_3{\cdot}9H_2O$ (Dinâmica®, 98.5% purity), and 1.292 g of SiO_2 (NEON, 98% purity). The proportions were obtained according to balanced ionic equation (Eq. 1) for the formation of β-spodumene. Following the mentioned ratio, 3.032 g of whey protein per sample were required.

$$LiNO_3 + Al(NO_3)_3.9H_2O + 2SiO_2 \rightarrow LiAlSi_2O_6 + 4HNO_3 + 7H_2O \quad (1)$$

The gel formation is induced by the acidic nature of the final suspension (pH = 4), facilitating the condensation

reactions of protein chains, which lead to the formation of a connected porous structure. Afterward, the gels were heated to 100 °C for 1 h with continuous stirring to remove excess water. Subsequently, they were dried in an oven at 100 °C for 48 h, yielding xerogels. These xerogels were then subjected to calcination in an alumina boat crucible (20 mL) at 700 °C for 2 h, with a heating rate of 5 °C/min, ensuring complete combustion of protein chains. Additional thermal treatment was used, involving temperatures ranging from 800 to 1100 °C for 2 h, in increments of 100 °C, at a heating rate of 10 °C/min, to promote the formation of the crystalline phase of β-spodumene. Samples were slowly cooled in a closed muffle furnace until reaching room temperature. Subsequently, the samples produced were homogenized in an agate mortar and then sieved through 100 mesh and 200 mesh sieves.

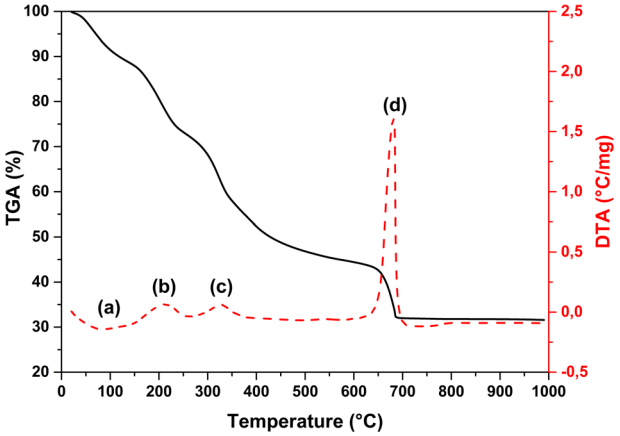

Fig. 1 TGA and DTA curves characteristics of the xerogel. An expressive mass loss in four different steps and stability above 700 °C are noticed

2.2 Characterization

The xerogel was initially analyzed using thermogravimetric analysis (TGA) and differential thermal analysis (DTA) to investigate the degradation pathways of organic chains and the formation of crystalline structures. TGA/DTA curves were obtained with a Q600/2960 thermogravimetric analyzer (TA Instruments), which was equipped with an automated gas flow controller. Powder samples were placed in alumina crucibles and heated from 25 °C to 1000 °C at a rate of 10 °C/min, under a synthetic air flow of 100 mL/min.

X-ray diffraction (XRD) measurements of the produced samples were performed using a powder diffractometer Miniflex (Rigaku), with Cu-Kα radiation ($\lambda = 1.5406$ Å) tube operated at 40 kV and 15 mA in continuous mode. XRD data were collected in a scan range of 10–90° (2θ), employing a scan speed of 10°/min with 0.02° step intervals at room temperature. Experimental patterns were compared with theoretical patterns from the PDF2 (Powder Diffraction File) crystallographic database to determine the positions and intensities of Bragg peaks and to identify references. This comparison was facilitated using X'Pert High Score Plus software (PANalytical B.V.). The quantitative confirmation of β spodumene single-phase formation in the produced samples was achieved by the Rietveld refinement method [31], employing the DBWSTools 2.4 program [32]. The Pseudo-Voigt function was applied to fit peak profiles of the identified crystalline phase. Quality factors of refinement were determined accordingly.

Fourier Transform Infrared Spectroscopy (FTIR) analysis was employed as a complementary technique to assess the crystallization process under different thermal treatments. Transmittance spectra were obtained utilizing a Spectrum 2 spectrometer (PerkinElmer), which was outfitted with a near-infrared source and a lithium tantalate ($LiTaO_3$) detector. Powder samples were compressed into thin pellets, measuring 7.0 mm in diameter and ~0.1 mm in thickness, within a potassium bromide (KBr) matrix at a ratio of 1 mg of sample to 30 mg of KBr. A continuous scan encompassed the spectral range from 450 cm^{-1} to 1200 cm^{-1} for all specimens.

Additionally, X-ray fluorescence (XRF) analysis was performed to ascertain the chemical composition of the samples and detect any contained impurities. The portable benchtop XRF analyzer CTX 800 (Bruker), equipped with a 50 kV, 4 W Rh-target excitation source and an SDD detector featuring a graphene window and detector shield, was employed to analyze elemental compositions. The samples were prepared as 15.0 mm diameter pellets using a high-purity PVA solution (0.02 g/mL) as a binder. The weight percentages in the form of oxides were determined.

3 Results and discussion

The TGA curve (Fig. 1) demonstrates an almost gradual mass loss up to 650 °C. However, some DTA peaks are observed within this range, corresponding to the following events: (a) an endothermic process of water evaporation around 100 °C; (b) denaturation of proteins or the breakdown of secondary and tertiary structures between 150 °C and 250 °C; and (c) the primary degradation of protein chains starting at 300 °C. Between 650 °C and 700 °C, a final event (d) is observed, corresponding to the oxidation of remaining organic residues, resulting in a final mass loss and the release of CO_2. The mass then stabilizes, indicating that the majority of the organic material has been decomposed. Therefore, it is suggested that during sample production, the calcination process aimed at eliminating organic constituents should be conducted at a minimum temperature of 700 °C. This temperature threshold results in an approximate cumulative mass loss of 70% and ensures

stability between 700 °C and 1000 °C, indicating the absence of residual organic matter. The events are similar to those observed during the degradation of gelatin-based xerogels for the synthesis of β-spodumene [4] and find support in the literature that evaluated the thermal decomposition of whey protein [33, 34].

Figure 2 shows the XRD patterns of samples produced at different thermal treatments. Experimental patterns were cross-referenced with the ICSD 14235 reference pattern, representing β-spodumene. For sample subjected to thermal treatment at 800 °C, the presence of peaks related to precursor phases, namely silicon dioxide (SiO_2) and eucryptite ($LiAlSiO_4$), is predominant. At 900 °C treatment, the presence of these peaks persists, albeit with some discernible β-spodumene peaks, indicating an incomplete conversion to β-spodumene. For samples treated from 1000 °C, the experimental patterns display identical crystalline structures, featuring well-defined peaks corresponding to the reference pattern ICSD 14235. When compared to methods relying solely on solid-state reactions, which commonly require temperatures above 1200 °C (some references are shown in Table 1), a significant reduction in the formation temperature of the β-spodumene phase was observed.

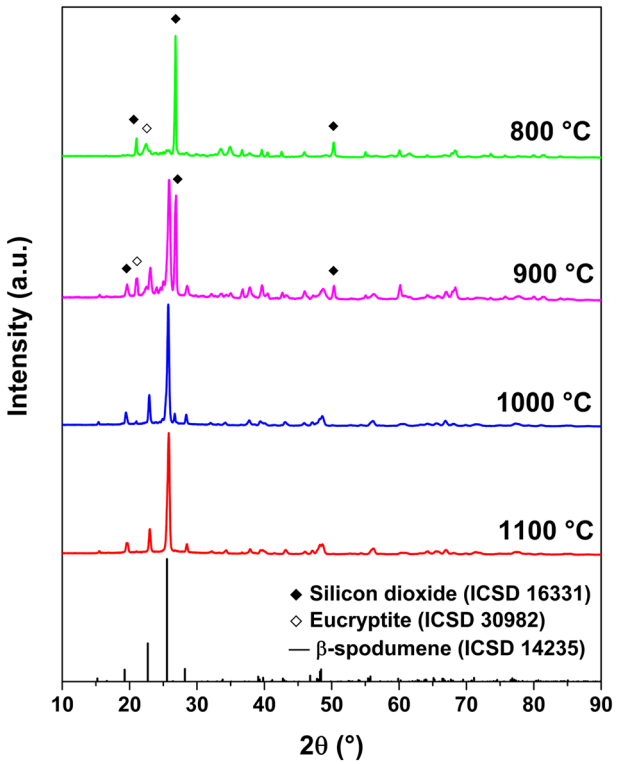

Fig. 2 XRD patterns of samples produced at different thermal treatments; the reference pattern of β-spodumene (ICSD 14235); and the minor phases reference phases of silicon dioxide (ICSD 16331) and eucryptite (ICSD 30982)

The Rietveld refinement adjustments, depicted in Fig. 3, were conducted specifically for the samples that effectively formed the β-spodumene phase (at heat-treatments of 1000 and 1100 °C, respectively). The disparity between the experimental and model-calculated values (I_{OBS}–I_{CALC}) was minimal, indicating a satisfactory fit between the observed and calculated intensities. The quality factors are provided as percentages: obtained error (R_{wp}), and expected error (R_e). The ratio R_{wp}/R_e, denoted as χ, is of significant importance. A value of χ close to 1 indicates a well-refined dataset where $R_{wp} \approx R_e$. Only values of $\chi \geq 1$ are plausible, and $\chi < 1.5$ is generally considered satisfactory [35]. Integrated intensity factors (R_B) are reported to assess the discrepancy between the observed diffraction peak intensities and the values calculated by the theoretical model [36]. The fitting quality factors, disclosed a precise fit by the method, as evidenced by the reduced error values obtained ($R_{wp} \approx 15\%$) and quality factors ($\chi \approx 1.2$). Moreover, integrated intensity factors exhibited acceptable values ($R_B \approx 10\%$), which demonstrates the model's adequacy. The synthesized β-spodumene crystallizes in the tetragonal system, with space group $P4_32_12$ and lattice parameters: $a = b = 7.534$ Å, $c = 9.158$ Å, $\alpha = \beta = \gamma = 90°$. This unit cell exhibits a density of 2.38 g/cm³ and a volume of 519.82 $Å^3$.

Table 1 Comparative characteristics of β-spodumene synthesis reported in the literature

Synthesis method [ref]	Heat-treatment parameters			Applications
	Heating rate (°C/min)	Temperature (°C)	Exposure time (h)	
Melting [39]	-	1425	-	Determination of the crystal structure
Solid-state reaction [10]	-	1480	2	Thermoluminescent dosimetry
Sol–gel/hot pressing [8]	-	1200–1350	0.5	Glass-ceramic composites manufacturing
Gelatin-assisted sol–gel [4]	10	800–1100	2	Thermoluminescent dosimetry
Solid-state reaction [9]	-	1200	2	Glass-ceramic composites manufacturing
Solid-state reaction [40]	-	1300	5	Down/up-conversion (DC/UC) luminescence
Solid-state reaction [41]	-	1200–1400	4	Synthesis and photoluminescence of near-infrared (NIR) phosphors
Gelatin-assisted sol–gel [6, 7]	10	1100	2	Ceramic pigments manufacturing

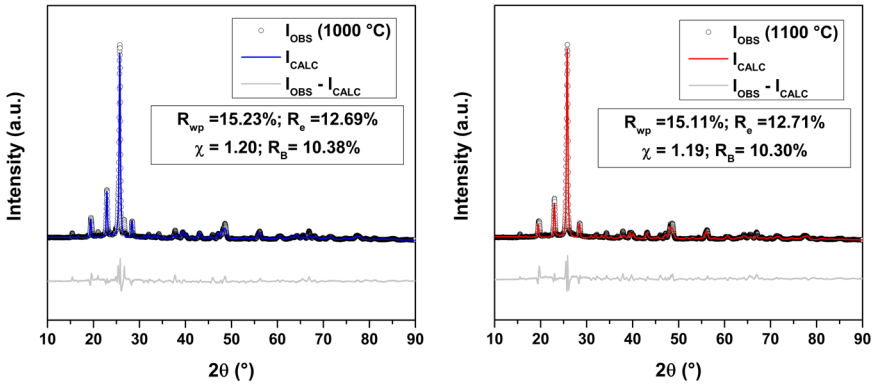

Fig. 3 XRD patterns of the samples treated at 1000 and 1100 °C (I_{OBS}), the fit calculated by Rietveld refinement (I_{CALC}), and the intensities difference ($I_{OBS} - I_{CALC}$)

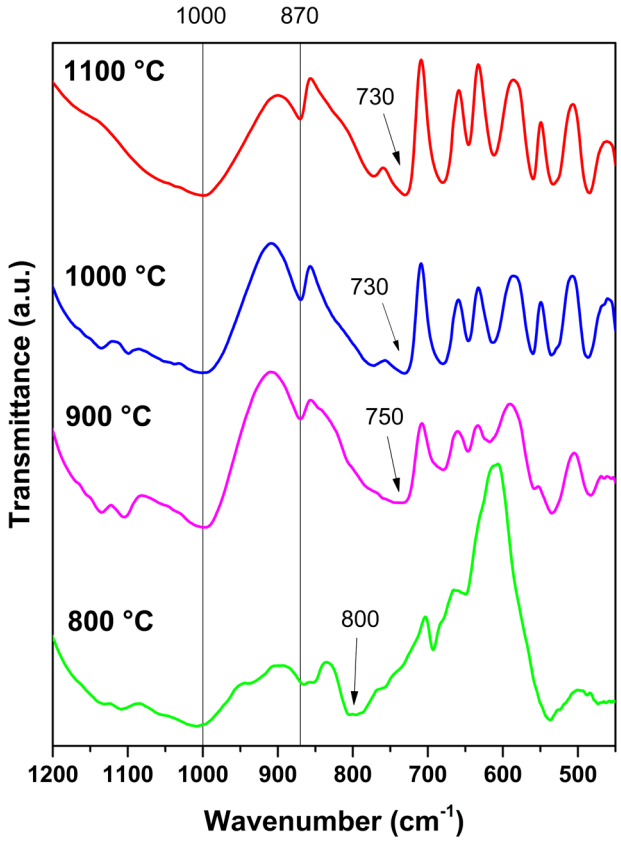

Fig. 4 FTIR spectra of samples produced at different thermal treatments

Figure 4 presents the FTIR spectra of samples produced at different thermal treatments. In all spectra, the strong broad band around 1000 cm^{-1} is associated with Si-O stretching vibration, while the region around 700 cm^{-1} corresponds to Al-O stretching vibration. An absorption band in the wavenumber region of 870 cm^{-1}, characteristic of AlO_6 octahedra, is also observed. However, a band shift is noted between 800 cm^{-1} and 730 cm^{-1} with increasing synthesis temperature, indicating a trend of AlO_4 tetrahedra substitution by SiO_4 through diffusion processes, facilitating β-spodumene formation. The tetrahedral arrangement of aluminum within spodumene arises from the inherent crystalline lattice structure of the mineral, in which aluminum and silicon share the same occupancy site in random positions. This band, around 750 cm^{-1}, indicates the characteristic vibration of the covalent Al-O bond in AlO_4 tetrahedra in spodumene and aluminum substitution in silica tetrahedra, supporting the crystallization results obtained by XRD. Furthermore, several sharp small peaks are observed in the region of 500–700 cm^{-1}, related to the bending of Si-O and Al-O bonds, while bands in the 400–500 cm^{-1} range refer to Si-O-Si bending and skeletal vibrations. These results are supported by the literature on infrared studies of β-spodumene produced by the sol–gel route [37, 38].

Table 2 presents the chemical composition of the samples produced under different thermal treatments, as determined using the XRF technique. It is noteworthy that the weight proportions of Al_2O_3 and SiO_2 closely align with the theoretical values corresponding to the stoichiometric structural formula of spodumene. However, the LiO_2 contents of the samples are unavailable due to the technique's limitation in detecting elements with low XRF energy. A significant residual sulfur (S) content is evident in the sample treated at 800 °C (3.07%), attributed to the post-combustion of protein chains. Nonetheless, this content notably decreases with increasing treatment temperature, reaching levels below the detection limit (<LOD) at 1100 °C, likely due to elimination by oxidation reactions in the form of SO_2 gas. This treatment temperature is recommended for complete removal of sulfur from the sample. The minor presence of P_2O_5, K_2O, and CaO (<1%) is likely attributed to impurities commonly found in whey protein. Fe_2O_3 (<0.1%) is commonly an impurity present in analytical chemical reagents.

Metallic impurities may potentially act as recombination centers in thermoluminescent (TL) applications of β-spodumene [10]. Therefore, this result requires further investigation with analyses of the TL emission curve of the material obtained by this method.

Table 2 Chemical composition of samples produced at different thermal treatments

Comp.	Theoretical (wt%)	800 °C	900 °C	1000 °C	1100 °C
LiO_2	8.03	-	-	-	-
Al_2O_3	27.4	27.28 ± 0.35	29.74 ± 0.37	29.42 ± 0.36	27.57 ± 0.35
SiO_2	64.6	65.16 ± 0.40	65.08 ± 0.36	66.52 ± 0.36	65.28 ± 0.35
P_2O_5	-	0.82 ± 0.04	0.96 ± 0.04	0.76 ± 0.04	0.65 ± 0.04
S	-	3.07 ± 0.03	1.92 ± 0.03	0.84 ± 0.02	<LOD
K_2O	-	0.95 ± 0.02	0.91 ± 0.02	0.91 ± 0.02	0.88 ± 0.01
CaO	-	0.74 ± 0.05	0.63 ± 0.04	0.68 ± 0.04	0.67 ± 0.04
Fe_2O_3	-	0.06 ± 0.01	0.05 ± 0.01	0.04 ± 0.01	0.04 ± 0.01

4 Conclusions

The study successfully synthesized β-spodumene using a new sol–gel method assisted by whey protein. The crystalline structure of β-spodumene was achieved at 1000 °C, marking a significant reduction in synthesis temperature compared to conventional solid-state methods. Additionally, the study demonstrated that sulfur (S) residues from protein chains can be effectively eliminated through heat-treatment at 1100 °C. β-spodumene crystallized in the tetragonal structure with the space group $P4_32_12$, characterized by lattice parameters $a = b = 7.534$ Å, $c = 9.158$ Å, and $\alpha = \beta = \gamma = 90°$, with a density of 2.38 g/cm³ and a volume of 519.82 Å^3.

The use of whey protein as a chelating agent represents a sustainable approach in the sol–gel synthesis of materials, highlighting its ecological potential. This research opens new avenues for exploring novel sol–gel methodologies in the synthesis of aluminosilicates and emphasizes the feasibility of using natural protein sources in materials science. Future research could explore more specific applications of β-spodumene produced by this innovative synthesis route.

Acknowledgements This work was supported by Coordination for the Improvement of Higher Education Personnel (CAPES), Brazilian Funding Agency for Studies and Projects (FINEP) and Pernambuco Science and Technology Support Foundation (FACEPE). The authors are also grateful for the support of collaborating educational institutions including Federal Institute of Sertão de Pernambuco (IFSertão-PE), Federal University of São Francisco Valley (Univasf) and University of São Paulo (USP).

Author contributions All authors contributed to the study conception and design. Material preparation, data collection and analysis were performed by Ricardo Ferrari Ferraz. The first draft of the manuscript was written by Ricardo Ferrari Ferraz and all authors commented on previous versions of the manuscript. All authors read and approved the final manuscript.

Compliance with ethical standards

Conflict of interest The authors declare no competing interests.

References

1. Mo Z, Su S, Huo Y et al. (2021) Hakeem, enhanced dual mode luminescence via energy transfer in Er^{3+}, Yb^{3+} co-doped β-spodumene J Alloy Compd 872:159551. https://doi.org/10.1016/j.jallcom.2021.159551
2. Alatishe MA, Ogundare FO, Folley DE et al. (2020) Optically stimulated luminescence and spectral emission features of radioluminescence and thermoluminescence of natural kunzite Radiat Meas 138:106457. https://doi.org/10.1016/j.radmeas.2020.106457
3. d'Amorim RAPO, de Vasconcelos DAA, de Barros VSM et al. (2014) Characterization of α-spodumene to OSL dosimetry Radiat Phys Chem 95:141–144. https://doi.org/10.1016/j.radphyschem.2013.01.029
4. Lima HRBR, Nascimento DS, Bispo GFC et al. (2014) Production and characterization of spodumene dosimetric pellets prepared by a sol–gel route Radiat Phys Chem 104:93–99. https://doi.org/10.1016/j.radphyschem.2014.03.022
5. Sardisco L, Hannula P-M, Pearce TJ, Morgan L (2022) Multitechnique analytical approach to quantitative analysis of spodumene. Minerals 12:175. https://doi.org/10.3390/min12020175
6. Ferraz RF, Sousa JF, Costa DS, et al. (2022) Development of a β-$LiAlSi_2O_6$:Cr-based ceramic pigment by proteic sol-gel process using gelatin: synthesis and characterization. Mater Res 25. https://doi.org/10.1590/1980-5373-MR-2021-0315
7. Ferrari Ferraz R, Ferreira Sousa J, Batista Reis Lima HR, Pessoa Oliveira RA (2022) Structural and morphological characterization of the chromium-doped β-spodumene to ceramic pigment. Braz J Radiat Sci 10. https://doi.org/10.15392/bjrs.v10i2A.1772
8. Xia L, Wang X, Wen G et al. (2012) Nearly zero thermal expansion of b-spodumene glass ceramics prepared by sol–gel and hot pressing method Ceram Int 38:5315–5318. https://doi.org/10.1016/j.ceramint.2012.03.004
9. Wang F, Chen X, Zhang W, Mao H (2018) Synthesis and characterization of borosilicate glass/β-spodumene/Al_2O_3 composites with low CTE value for LTCC applications. J Mater Sci Mater Electron 29:9038–9044. https://doi.org/10.1007/s10854-018-8929-z
10. Ferraz GM, Paião JRB, Watanabe S, Souza SO (2008) Synthetic spodumene polycrystals as a TL dosimetric material. Radiat Meas 43:387–391. https://doi.org/10.1016/j.radmeas.2007.11.026
11. Navas D, Fuentes S, Castro-Alvarez A, Chavez-Angel E (2021) Review on sol-gel synthesis of perovskite and oxide nanomaterials. Gels 7. https://doi.org/10.3390/gels7040275
12. Parashar M, Shukla V, Singh R (2020) Metal oxides nanoparticles via sol–gel method: a review on synthesis, characterization and applications. J Mater Sci: Mater Electron 31:3729–3749. https://doi.org/10.1007/s10854-020-02994-8
13. Lima HRBR, Nascimento DS, Sussuchi EM et al. (2017) Synthesis of MgB_4O_7 and $Li_2B_4O_7$ crystals by proteic sol–gel and

Pechini methods J Sol-Gel Sci Technol 81:797–805. https://doi.org/10.1007/s10971-016-4249-z
14. Bokov D, Turki Jalil A, Chupradit S et al. (2021) Nanomaterial by sol-gel method: synthesis and application Adv Mater Sci Eng 2021:1–21. https://doi.org/10.1155/2021/5102014
15. Marami MB, Farahmandjou M, Khoshnevisan B (2018) Sol–gel synthesis of Fe-doped TiO_2 nanocrystals. J Electron Mater 47:3741–3748. https://doi.org/10.1007/s11664-018-6234-5
16. Chakraborty A, Naskar MK (2022) Sol–gel synthesis of alumina gel zeolite X nanocomposites for high performance water defluoridation: batch and column adsorption study. Mater Adv 3:8544–8556. https://doi.org/10.1039/d2ma00392a
17. Shichalin OO, Papynov EK, Nepomnyushchaya VA et al. (2022) Hydrothermal synthesis and spark plasma sintering of NaY zeolite as solid-state matrices for cesium-137 immobilization J Eur Ceram Soc 42:3004–3014. https://doi.org/10.1016/j.jeurceramsoc.2022.02.007
18. Yarusova SB, Shichalin OO, Belov AA et al. (2022) Synthesis of amorphous $KAlSi_3O_8$ for cesium radionuclide immobilization into solid matrices using spark plasma sintering technique Ceram Int 48:3808–3817. https://doi.org/10.1016/j.ceramint.2021.10.164
19. Dran'kov A, Shichalin O, Papynov E (2022) Hydrothermal synthesis, structure and sorption performance to cesium and strontium ions of nanostructured magnetic zeolite composites. Nucl Eng Technol 54:1991–2003. https://doi.org/10.1016/j.net.2021.12.010
20. Lucas JMF, Soreto Teixeira S, Gavinho SR et al. (2019) Niobium oxide prepared by sol–gel using powder coconut water J Mater Sci Mater Electron 30:11346–11353. https://doi.org/10.1007/s10854-019-01482-y
21. Gomes MA, Brandão-Silva AC, Avila JFM et al. (2018) Particle size effect on structural and optical properties of Y2O3:Nd3+ nanoparticles prepared by coconut water-assisted sol-gel route J Lumin 200:43–49
22. Sampaio DV, Silva MS, Souza NRS et al. (2018) Electrical characterization of $BaTiO_3$ and $Ba_{0.77}Ca_{0.23}TiO_3$ ceramics synthesized by the proteic sol–gel method Ceram Int 44:15526–15530. https://doi.org/10.1016/j.ceramint.2018.05.213
23. Gomes P, Costa B, Carvalho JPF, et al. (2023) Cobalt Ferrite synthesized using a biogenic sol–gel method for biomedical applications. Molecules 28. https://doi.org/10.3390/molecules28237737
24. Zak AK, Esmaeilzadeh J, Hashim AM (2024) Exploring the gelatin-based sol-gel approach: a convenient route for fabricating high-quality pure and doped ZnO nanostructures. Ceram Int 50:12649–12663. https://doi.org/10.1016/j.ceramint.2024.01.254
25. Yazdi ST, Mousavi M, Khorrami GH (2021) Effect of Co-doping in V_2O_5 nanoparticles synthesized via a gelatin-based sol-gel method. Mater Today Commun 26:101955. https://doi.org/10.1016/j.mtcomm.2020.101955
26. Pires AF, Marnotes NG, Rubio OD, et al. (2021) Dairy by-products: a review on the valorization of whey and second cheese whey. Foods 10. https://doi.org/10.3390/foods10051067
27. Siso MIG (1996) The biotechnological utilization of cheese whey: a review. Bioresour Technol 57:1–11. https://doi.org/10.1016/0960-8524(96)00036-3
28. Buchanan D, Martindale W, Romeih E, Hebishy E (2023) Recent advances in whey processing and valorisation: technological and environmental perspectives. Int J Dairy Technol 76:291–312. https://doi.org/10.1111/1471-0307.12935
29. Carvalho F, Prazeres AR, Rivas J (2013) Cheese whey wastewater: characterization and treatment. Sci Total Environ 445-446:385–96. https://doi.org/10.1016/j.scitotenv.2012.12.038
30. Soares VA, Xavier MJS, Rodrigues ES et al. (2020) Green synthesis of ZnO nanoparticles using whey as an effective chelating agent Mater Lett 259:126853. https://doi.org/10.1016/j.matlet.2019.126853
31. Rietveld HM (1969) A profile refinement method for nuclear and magnetic structures. J Appl Crystallogr 2:65–71. https://doi.org/10.1107/S0021889869006558
32. Bleicher L, Sasaki JM, Santos COP (2000) Development of a graphical interface for the Rietveld refinement program DBWS J Appl Crystallogr 33:1189. https://doi.org/10.1107/S0021889800005410
33. Caetano-Silva ME, Alves RC, Lucena GN et al. (2017) Synthesis of whey peptide-iron complexes: influence of using different iron precursor compounds. Food Res Int 101:73–81. https://doi.org/10.1016/j.foodres.2017.08.056
34. Volić M, Pećinar I, Micić D et al. (2022) Design and characterization of whey protein nanocarriers for thyme essential oil encapsulation obtained by freeze-drying Food Chem 386:132749. https://doi.org/10.1016/j.foodchem.2022.132749
35. Pince E (1993) In: Young RA (ed) The Rietveld method. Oxford University Press, Oxford
36. David WIF (2004) On the equivalence of the Rietveld method and the correlated integrated intensities method in powder diffraction. J Appl Crystallogr 37:621–628. https://doi.org/10.1107/S0021889804013184
37. Covino J, De Laat FGA, Welsbie RA (1986) Synthesis and preliminary processing of the sol-gel derived β-quartz lithium aluminum silicates. J Non-Cryst Solids 82:329–342. https://doi.org/10.1016/0022-3093(86)90149-3
38. Xia L, Wen G, Song L (2009) Sol–gel synthesis and crystallization behaviour of β-spodumene. J Sol-Gel Sci Technol 52:134–139. https://doi.org/10.1007/s10971-009-2001-7
39. Li CT, Peacor DR (1968) The crystal structure of $LiAlSi_2O_6$-II ("β spodumene"). Z Krist 126:46–65. https://doi.org/10.1524/zkri.1968.126.1-3.46
40. Mo Z, Su S, Huo Y et al. (2021) Hakeem, Enhanced dual mode luminescence via energy transfer in Er^{3+}, Y b^{3+} co-doped β-spodumene J Alloy Compd 872:159551. https://doi.org/10.1016/j.jallcom.2021.159551
41. Yuan Z, Li G, Zhou M et al. (2022) Synthesis, structure and photoluminescence properties of NIR phosphor $LiAlSi_2O_6:Cr^{3+}$ Opt Mater 134:113124. https://doi.org/10.1016/j.optmat.2022.113124